Eur. Phys. J. A **21**, 507–520 (2004)
DOI 10.1140/epja/i2004-10004-2

THE EUROPEAN PHYSICAL JOURNAL A

Near-threshold production of $a_0(980)$-mesons in the reaction $pp \to dK^+\bar{K}^0$

V.Yu. Grishina[1], L.A. Kondratyuk[2], M. Büscher[3,a], and W. Cassing[4]

[1] Institute for Nuclear Research, 60th October Anniversary Prospect 7A, 117312 Moscow, Russia
[2] Institute of Theoretical and Experimental Physics, B. Cheremushkinskaya 25, 117259 Moscow, Russia
[3] Institut für Kernphysik, Forschungszentrum Jülich, D-52425 Jülich, Germany
[4] Institut für Theoretische Physik, Universität Giessen, Heinrich-Buff-Ring 16, D-35392 Giessen, Germany

Received: 26 February 2004 /
Published online: 21 September 2004 –
Communicated by V.V. Anisovich

Abstract. Using an effective Lagrangian approach as well as the Quark-Gluon Strings Model, we analyze near-threshold production of $a_0(980)$-mesons in the reaction $NN \to dK\bar{K}$ as well as the background of non-resonant $K\bar{K}$-pair production. We argue that the reaction $pp \to dK^+\bar{K}^0$ at an energy release $Q \leq 100\,\mathrm{MeV}$ is dominated by the intermediate production of the $a_0(980)$-resonance. At larger energies the non-resonant $K^+\bar{K}^0$-pair production —where the kaons are produced in a relative P-wave— becomes important. The effects of final-state interactions are evaluated in a unitarized scattering length approach and found to be in the order of a 20% suppression close to threshold. Thus, in present experiments at the Cooler Synchrotron COSY-Jülich for $Q \leq 107\,\mathrm{MeV}$ the a_0^+ signal can reliably be separated from the non-resonant $K^+\bar{K}^0$ background.

PACS. 25.10.+s Nuclear reactions involving few-nucleon systems – 13.75.-n Hadron-induced low- and intermediate-energy reactions and scattering (energy $\leq 10\,\mathrm{GeV}$)

1 Introduction

During the last two decades, the physics of the lightest scalar mesons $a_0(980)$ and $f_0(980)$ has gained vivid attention. The constituent quark model considers these scalar mesons as conventional $q\bar{q}$ states (see, *e.g.*, refs. [1–5] and references therein); however, the structure of these states seems to be more subtle. Alternative descriptions are $K\bar{K}$ molecules [6–8], unitarized $q\bar{q}$ states [9,10] or four-quark cryptoexotic states [11–13]. A further problem with these light scalar mesons is a possibly strong mixing between the uncharged $a_0(980)$ and the $f_0(980)$ due to a common coupling to $K\bar{K}$ intermediate states [12,14–16]. This effect will influence the structure of the uncharged component of the $a_0(980)$ and implies that a comparative study of the a_0^0 and a_0^+ (or a_0^-) has to be performed. Moreover, the $a_0(980)$-$f_0(980)$ mixing can generate isospin violation in different reactions with a_0/f_0 production [17–20].

At COSY-Jülich an experimental program on the study of near-threshold a_0/f_0 production in pp, pn, pd and dd interactions has been started with the ANKE spectrometer [21–25]. Recently, first results on the reaction $pp \to dK^+\bar{K}^0$ near threshold have become available at an excess energy of $Q = 46\,\mathrm{MeV}$ [26]. The present study is devoted to the theoretical analysis of these data. Furthermore, we provide predictions for different observables at larger excess energy Q and investigate the influence of final-state interactions (FSI), the importance of which has been pointed out in ref. [27].

In a recent work [28], we have considered a_0 production in the reactions $\pi N \to a_0 N$ and $NN \to da_0$ near threshold and at beam energies up to a few GeV. An effective Lagrangian approach as well as the Regge-pole model were applied to investigate different contributions to the cross-section of the reaction $\pi N \to a_0 N$. These results were also used for an analysis of a_0 production in NN collisions [29,30]. In this paper we present a more detailed study of the reaction $NN \to dK\bar{K}$, taking into account both the a_0 contribution to this reaction and the non-resonant $K\bar{K}$ background. We demonstrate that the u-channel mechanism —normalised to the data from LBL (Berkeley) for the reaction $pp \to dX$ at $3.8\,\mathrm{GeV}/c$ [31]— can reproduce the total cross-section of the reaction $pp \to da_0^+ \to dK^+\bar{K}^0$ at $3.46\,\mathrm{GeV}/c$ ($Q = 46\,\mathrm{MeV}$) as measured at ANKE. However, it fails to reproduce the distribution in the deuteron scattering angle. We show that quantitatively better results can be achieved within the framework of the Quark-Gluon Strings Model (QGSM).

[a] e-mail: m.buescher@fz-juelich.de

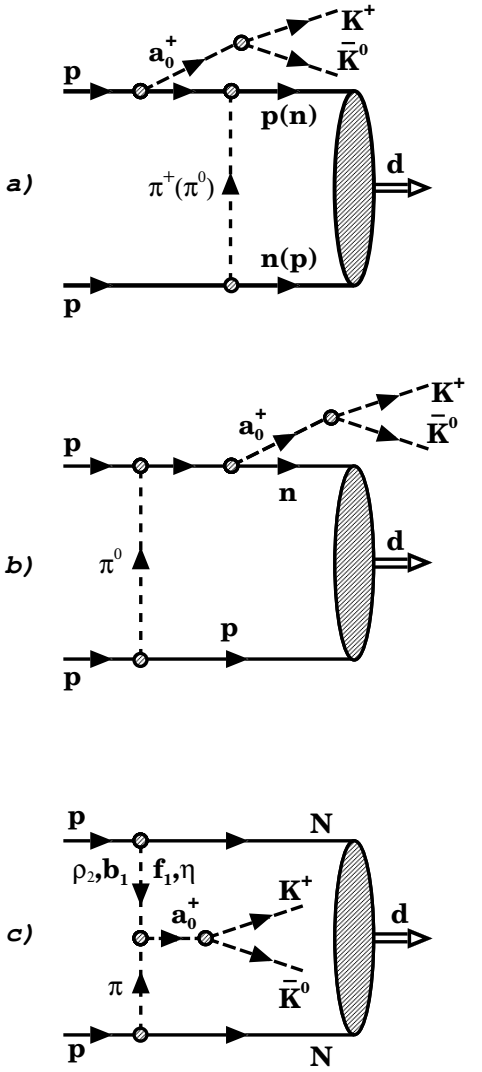

Fig. 1. Diagrams describing resonant contributions to the reaction $pp \to dK^+\bar{K}^0$ within the framework of the two-step model.

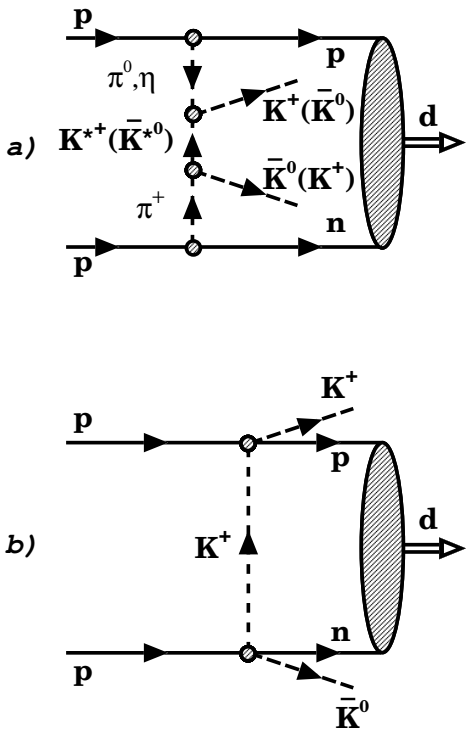

Fig. 2. Diagrams describing non-resonant mechanisms in the reaction $pp \to dK^+\bar{K}^0$ within the framework of the two-step model.

Our paper is organized as follows: In sects. 2 and 3 the two-step model within the framework of an effective Lagrangian approach is used for the analysis of different contributions for resonant (through the a_0) and non-resonant production of $K\bar{K}$ pairs in the reaction $NN \to dK\bar{K}$. In sect. 4 the reaction $NN \to da_0 \to dK\bar{K}$ is considered additionally within the Quark-Gluon Strings Model, while in sect. 5 a detailed analysis of final-state interactions (FSI) is given. Our conclusions are presented in sect. 6. The amplitudes for the different contributions to the reactions $\pi N \to a_0 N$ are given in the appendix.

2 Effective Lagrangian approach to the reaction NN → dK$\bar{K}$

Within the framework of the two-step model (TSM) with one-pion exchange in the intermediate state (cf. refs. [32, 33]) the contributions of hadronic intermediate states to the amplitude of the reaction $pp \to da_0^+ \to dK^+\bar{K}^0$ are described by diagrams *a*)-*c*) in fig. 1. Accordingly, we consider different contributions to the resonant amplitude $\pi N \to a_0 N \to K\bar{K}N$:
i) the u- and s-channel nucleon exchanges (fig. 1a) and b), respectively);
ii) the η- and $f_1(1285)$-meson exchanges (fig. 1c);
iii) the b_1- and ρ_2-Reggeon exchanges (fig. 1c).
The non-resonant background contribution to the reaction $NN \to dK\bar{K}$ is described by the diagrams in fig. 2a) and b) for $\pi - K^\star - \pi(\eta)$- and K-exchange, respectively (see also ref. [30]).

Since we are interested in the $pp \to da_0^+$ and $pp \to dK^+\bar{K}^0$ cross-sections near threshold, where the momentum of the final deuteron is comparatively small, we use a non-relativistic description of this particle by neglecting the 4th component of its polarization vector. Correspondingly, the relative motion of the nucleons in the deuteron is also treated non-relativistically. The $pp \to da_0^+$ and $pp \to dK^+\bar{K}^0$ amplitudes have to be antisymmetrized with respect to permutation of the initial protons a and b and therefore can be written as

$$T_{pp\to da_0^+}(\mathbf{p}_a, \mathbf{q}_d) = T^{ab}_{pp\to da_0^+}(\mathbf{p}_a, \mathbf{q}_d) - T^{ba}_{pp\to da_0^+}(\mathbf{p}_b, \mathbf{q}_d), \quad (1)$$

$$T_{pp\to dK^+\bar{K}^0}(\mathbf{p}_a, \mathbf{q}_d, \mathbf{q}_{12}) = T^{ab}_{pp\to dK^+\bar{K}^0}(\mathbf{p}_a, \mathbf{q}_d, \mathbf{q}_{12}) - T^{ba}_{pp\to dK^+\bar{K}^0}(\mathbf{p}_b, \mathbf{q}_d, \mathbf{q}_{12}). \quad (2)$$

Here and below the notations q_1, q_2, q_d, p_a and p_b are used for the 4-momenta of the $\bar{K}^0$, K^+, deuteron, initial protons a and b, respectively. We have introduced the relative 3-momentum $\mathbf{q}_{12} = (\mathbf{q}_1 - \mathbf{q}_2)/2$ for the final kaons, which are also considered as non-relativistic particles for excess energies $Q \leq 100$–$150\,\mathrm{MeV}$. The motion of the nucleons a' and b' in the deuteron is described by the relative momentum $\mathbf{p}_{b'a'} \equiv (\mathbf{p}_{b'} - \mathbf{p}_{a'})/2 = \mathbf{p}_{b'} - \mathbf{q}_d/2$. Then one can write the first terms $T^{ab}_{pp\to da_0^+}(\mathbf{p}_a, \mathbf{q}_d)$ and $T^{ab}_{pp\to dK^+\bar{K}^0}(\mathbf{p}_a, \mathbf{q}_d, \mathbf{q}_{12})$ on the r.h.s. of eqs. (1) and (2) as [32]

$$T^{ab}_{pp\to da_0^+}(\mathbf{p}_a, \mathbf{q}_d) = \frac{f_{\pi NN}}{m_\pi}\big(p^0 + m_N\big)(2m_N)^{3/2} \times \sum_{X(a_0)} M^{\{X(a_0)\}\,jl}_{pp\to da_0^+}(\mathbf{p}_a, \mathbf{q}_d)\ \varphi^T_{\lambda_a}(\mathbf{p}_a) \times(-i\sigma_2)\sigma^j \boldsymbol{\sigma}\cdot\boldsymbol{\epsilon}^{*(d)}\sigma^l \varphi_{\lambda_b}(\mathbf{p}_b), \quad (3)$$

$$T^{ab}_{pp\to dK^+\bar{K}^0}(\mathbf{p}_a, \mathbf{q}_d, \mathbf{q}_{12}) = \frac{f_{\pi NN}}{m_\pi}\big(p^0 + m_N\big)(2m_N)^{3/2} \times \sum_{X} M^{\{X\}\,jl}_{pp\to dK^+\bar{K}^0}(\mathbf{p}_a, \mathbf{q}_d, \mathbf{q}_{12})\ \varphi^T_{\lambda_a}(\mathbf{p}_a) \times(-i\sigma_2)\sigma^j \boldsymbol{\sigma}\cdot\boldsymbol{\epsilon}^{*(d)}\sigma^l \varphi_{\lambda_b}(\mathbf{p}_b), \quad (4)$$

where $\mathbf{p}_a = -\mathbf{p}_b = \mathbf{p}$, $p^0 = p^0_a = p^0_b = \sqrt{\mathbf{p}^2 + m_N^2}$ in the center-of-mass frame. The tensor functions $M^{\{X(a_0)\}\,jl}_{pp\to da_0^+}(\mathbf{p}_a, \mathbf{q}_d)$ and $M^{\{X\}\,jl}_{pp\to dK^+\bar{K}^0}(\mathbf{p}_a, \mathbf{q}_d, \mathbf{q}_{12})$ are defined by the integrals

$$M^{\{X(a_0)\}\,jl}_{pp\to da_0^+}(\mathbf{p}_a, \mathbf{q}_d) = \int \frac{\mathrm{d}^3 p_{b'a'}}{(2\pi)^{3/2}}\ \Psi_d(\mathbf{p}_{b'a'}) \times\left\{-\frac{p_a^j}{p^0 + m_N} + \frac{(-2\,p_{b'a'} + q_d)^j}{4\,m_N}\right\} \times\Phi^{\{X(a_0)\}\,l}_{\pi N\to a_0 N}(\mathbf{p}_a, \mathbf{q}_d, \mathbf{p}_{b'a'})\ \frac{F_{\pi NN}(t_{aa'})}{t_{aa'} - m_\pi^2}\,, \quad (5)$$

$$M^{\{X\}\,jl}_{pp\to dK^+\bar{K}^0}(\mathbf{p}_a, \mathbf{q}_d, \mathbf{q}_{12}) = \int \frac{\mathrm{d}^3 p_{b'a'}}{(2\pi)^{3/2}}\ \Psi_d(\mathbf{p}_{b'a'}) \times\left\{-\frac{p_a^j}{p^0 + m_N} + \frac{(-2\,p_{b'a'} + q_d)^j}{4\,m_N}\right\} \times\Phi^{\{X\}\,l}_{\pi N\to K\bar{K}N}(\mathbf{p}_a, \mathbf{q}_d, \mathbf{q}_{12}, \mathbf{p}_{b'a'})\ \frac{F_{\pi NN}(t_{aa'})}{t_{aa'} - m_\pi^2}\,. \quad (6)$$

Here $\Psi_d(\mathbf{p}_{b'a'})$ is the deuteron wave function, $t_{aa'} = (p_a - p_{a'})^2$ is the virtual pion momentum squared. The vector functions

$$\Phi^{\{X(a_0)\}\,l}_{\pi N\to a_0 N}(\mathbf{p}_a, \mathbf{q}_d, \mathbf{p}_{b'a'})$$

and

$$\Phi^{\{X\}\,l}_{\pi N\to K\bar{K}N}(\mathbf{p}_a, \mathbf{q}_d, \mathbf{q}_{12}, \mathbf{p}_{b'a'})$$

depend on the mechanisms $X(a_0)$ (or X) of the a_0 (or $K\bar{K}$) production. For each vertex with a virtual meson we use the monopole form factor

$$F_j(t) = \frac{\Lambda_j^2 - m_j^2}{\Lambda_j^2 - t}\,, \quad (7)$$

where the Λ_j denote a cut-off parameter, $\Lambda_\pi = 1.3\,\mathrm{GeV}$.

In the case of $K\bar{K}$ production via a_0-resonance we have the well-known convolution formula

$$\Phi^{\{X(a_0)\}\,l}_{\pi N\to K\bar{K}N}(\mathbf{p}_a, \mathbf{q}_d, \mathbf{q}_{12}, \mathbf{p}_{b'a'}) = \Phi^{\{X(a_0)\}\,l}_{\pi N\to a_0 N}(\mathbf{p}_a, \mathbf{q}_d, \mathbf{p}_{b'a'}) \times F_0(m_{a_0}), \quad (8)$$

where $F_0(m_{a_0})$ is the Flatté mass distribution amplitude (see, *e.g.*, ref. [34]), $m_{a_0} = \sqrt{(q_1 + q_2)^2}$ and

$$\begin{aligned}\Phi^{\{X(a_0)\}\,l}_{\pi N\to K^+\bar{K}^0 N}(\mathbf{p}_a, \mathbf{q}_d, \mathbf{p}_{b'a'}) = {}& I^{\{X(a_0)\}}\ \left\{\left[-\frac{p_b^l}{p^0 + m_N} + \frac{(2\,p_{b'a'} + q_d)^l}{4\,m_N}\right]\right. \\ &\times A^{\{X(a_0)\}}\big(s_{\{a_0,\,b'\}}, t_{bb'}\big) \\ &+\left[p_b^l\left(\frac{q^0_{a_0} + m_N + \frac{\mathbf{p}_{b'a'}\cdot\mathbf{q}_d}{2m_N}}{p^0 + m_N}\right)\right. \\ &\quad + p^l_{b'a'}\left(\frac{q^0_{a_0} - m_N + \frac{\mathbf{p}_b\cdot\mathbf{q}_d}{p^0 + m_N}}{2m_N}\right) \\ &\quad \left.\left. + q_d^l\left(\frac{q^0_{a_0} + 3m_N - \frac{\mathbf{p}_b\cdot\mathbf{p}_{b'a'}}{p^0 + m_N}}{4m_N}\right)\right] \right. \\ &\left.\times B^{\{X(a_0)\}}\big(s_{\{a_0,\,b'\}}, t_{bb'}\big)\ \right\}. \end{aligned} \quad (9)$$

Here $I^{\{X(a_0)\}}$ denotes the isospin factor,

$$s_{\{a_0,\,b'\}} = (q_{a_0} + p_{b'})^2, \qquad t_{bb'} = (p_b - p_{b'})^2 \quad (10)$$

and the 4-momentum of the a_0 is defined as $q_{a_0} = p_a + p_b - q_d$. Two invariant amplitudes

$$A^{\{X(a_0)\}}\big(s_{\{a_0,\,b'\}}, t_{bb'}\big) \quad (11)$$

and

$$B^{\{X(a_0)\}}\big(s_{\{a_0,\,b'\}}, t_{bb'}\big) \quad (12)$$

define the s-channel helicity amplitudes for the $\pi N \to a_0 N$ reaction as follows [14]:

$$M_{\lambda_{b'}\lambda_b}(\pi^- p \to a_0 N) = \bar{u}_{\lambda_{b'}}\gamma_5\left\{-A(s,t) - \frac{1}{2}\,\gamma^\mu\,(q_\pi + q_{a_0})_\mu\,B(s,t)\right\}u_{\lambda_b}\,. \quad (13)$$

The amplitudes for different mechanisms of the $\pi^- p \to a_0 N$ reactions are given in the appendix for completeness. In the case of the s-, u-channel nucleon exchanges as well as ρ_2-, b_1-Reggeon exchanges, we fix the parameters of the invariant amplitudes $A(s,t)$ and $B(s,t)$ using the $\pi^- p \to a_0^0 n$ channel. Since the isoscalar η and f_1-exchange mechanisms do not contribute to this reaction, we choose the $\pi^- p \to a_0^- p$ channel to define parameters of the amplitudes $A(s,t)$ and $B(s,t)$. Then we can fix the isospin coefficients for different mechanisms in eq. (9) as follows: $I^{\{u\}} = 3$, $I^{\{s\}} = 1$, $I^{\{\rho_2\}} = I^{\{b_1\}} = 2$, $I^{\{\eta\}} = I^{\{f_1(1285)\}} = \sqrt{2}$.

The non-resonant $K\bar{K}$ production via $K^\star - P$-exchange with a pseudoscalar meson $P = \pi^0$ or η is given by

$$\Phi^{\{K^\star - P\}\ l}_{\pi N \to K\bar{K}N}(\mathbf{p}_a, \mathbf{q}_d, \mathbf{q}_{12}, \mathbf{p}_{b'a'}) = \frac{F_{PNN}(t_{bb'})}{t_{bb'} - m_P^2}\sqrt{2}\ T_{\pi^+P\to K^+\bar{K}^0}(\mathbf{p}_a, \mathbf{q}_d, \mathbf{q}_{12}, \mathbf{p}_{b'a'}) \times \left\{ -\frac{p_b^l}{p^0 + m_N} + \frac{(2\,p_{b'a'} + q_d)^l}{4\,m_N} \right\}, \quad (14)$$

where the elementary $\pi^+P \to K^+\bar{K}_0$ transition amplitude has the form

$$T_{\pi^+P\to K^+\bar{K}^0}(\mathbf{p}_a, \mathbf{q}_d, \mathbf{q}_{12}, \mathbf{p}_{b'a'}) = g_{K^\star\pi K} g_{K^\star PK}\sqrt{2} \times \left\{ (p_a - p_{a'} + q_1)_\mu (p_b - p_{b'} + q_2)^\mu \frac{(t_{aa'} - m_K^2)(t_{bb'} - m_K^2)}{m_{K^\star}{}^2} \right\} \times \frac{F_{\pi KK^\star}(t_{aa'}) F_{K^\star\pi K}(t_{K^\star}) F_{K^\star PK}(t_{K^\star}) F_{PKK^\star}(t_{bb'})}{t_{K^\star} - m_{K^\star}{}^2}. \quad (15)$$

Here $t_{K^\star} = (p_a - p_b - p_{a'} + p_{b'})^2$. The coupling constants $g_{K^\star\pi K} = -3.02$, $g_{K^\star\eta K} = \sqrt{3}\ g_{K^\star\pi K}$ and the cut-off parameter for the virtual $K^\star$-exchange $\Lambda_{K^\star}(K^\star\eta K) = 3.29\,\mathrm{GeV}$ are taken from ref. [7]. The remaining cut-off parameter $\Lambda_{K^\star}(K^\star\pi K)$ is adjusted to reproduce the experimental data [26] (see sect. 3). We note that amplitude (15) takes into account only the $K^{\star+}$-exchange. In the case of the $P = \pi(\eta)$ we should subtract (add) the corresponding $\bar{K}^{\star 0}$-exchange amplitude (obtained by the substitution $q_1 \leftrightarrow q_2$ in eq. (15)). This rule follows from G-parity conservation. We recall that the G-parity of the $K\bar{K}$-system with orbital momentum L and isospin I is given by $(-1)^{L+I}$. Therefore, for $I = 1$ in our case the orbital momentum of the $K\bar{K}$-pair should be odd for positive G-parity and even for negative G-parity. Thus, the non-resonant S-, D-... wave $K\bar{K}$-pair production in the $pp \to dK^+\bar{K}^0$ reaction is contributed by the $\pi - K^\star - \eta$-exchange mechanism (see also sect. 3). The non-resonant $\pi - K^\star - \pi$-exchange part of the $pp \to dK^+\bar{K}^0$ amplitude near threshold leads to P-, F-... wave $K\bar{K}$-pair production.

For the sake of completeness we have calculated also the K-exchange term defined by the diagram of fig. 1e). The corresponding amplitude reads

$$T^{\{K\}ab}_{pp\to dK^+\bar{K}^0}(\mathbf{p}_a, \mathbf{q}_d, \mathbf{q}_{12}) = \frac{1}{\sqrt{2m_N}} \times M^{\{K\}}_{pp\to dK^+\bar{K}^0}(\mathbf{p}_a, \mathbf{q}_d, \mathbf{q}_{12})\ \varphi^T_{\lambda_a}(\mathbf{p}_a)\ (-i\sigma_2)\boldsymbol{\sigma}\cdot\boldsymbol{\epsilon}^{*(d)}\varphi_{\lambda_b}(\mathbf{p}_b) \quad (16)$$

with the scalar function

$$M^{\{K\}}_{pp\to dK^+\bar{K}^0}(\mathbf{p}_a, \mathbf{q}_d, \mathbf{q}_{12}) = \int \frac{\mathrm{d}^3 p_{b'a'}}{(2\pi)^{3/2}}\ \Psi_d(\mathbf{p}_{b'a'}) \times A_{KN\to KN}(\mathbf{p}_a, \mathbf{q}_d, \mathbf{q}_{12})\ A_{\bar{K}N\to\bar{K}N}(\mathbf{p}_a, \mathbf{q}_d, \mathbf{q}_{12}) \times \frac{F^2_{KNN}(t_K)}{t_K - m_K^2}. \quad (17)$$

Here t_K is the squared 4-momentum of the virtual kaon. For the $KN(\bar{K}N)$ cross-sections we used the parametrizations from ref. [35]. The cut-off parameter Λ_K was taken to be 1.2 GeV (see, *e.g.*, ref. [36]).

Keeping in mind that the nucleons in the deuteron are considered as non-relativistic particles, the momentum transfers squared in the denominators of the propagators in eqs. (5), (9) can be rewritten as follows:

$$\begin{aligned} t_{aa'} &\simeq -2\left(p^0 - m_N\right)\ m_N - \frac{p^0}{m_N}\ \left(-\mathbf{p}_{b'a'} + \frac{\mathbf{q}_d}{2}\right)^2 \\ &\quad -2\mathbf{p}_a\cdot\mathbf{p}_{\,b'a'} + \mathbf{p}_a\cdot\mathbf{q}_d\,, \\ t_{bb'} &\simeq -2\left(p^0 - m_N\right)\ m_N - \frac{p^0}{m_N}\ \left(\mathbf{p}_{b'a'} + \frac{\mathbf{q}_d}{2}\right)^2 \\ &\quad -2\mathbf{p}_a\cdot\mathbf{p}_{\,b'a'} - \mathbf{p}_a\cdot\mathbf{q}_d\,, \\ t_{K^\star} &\simeq t_K \simeq -\left(\mathbf{p}_a + \mathbf{p}_{\,b'a'} - \mathbf{q}_{12}\right)^2. \end{aligned} \quad (18)$$

The structure of the amplitudes (1) and (2) guarantees that their S-wave parts (when the initial and final states have orbital momenta equal to zero) vanish, since they are forbidden by angular momentum conservation and the Pauli principle. The second terms $T^{ba}_{pp\to da_0^+}(\mathbf{p}_b, \mathbf{q}_d)$ and $T^{ba}_{pp\to dK^+\bar{K}^0}(\mathbf{p}_b, \mathbf{q}_d, \mathbf{q}_{12})$ on the r.h.s. of eqs. (1) and (2) can be obtained from the first ones $T^{ab}_{pp\to da_0^+}(\mathbf{p}_a, \mathbf{q}_d)$ in eq. (3) and $T^{ab}_{pp\to dK^+\overline{K}^0}(\mathbf{p}_a, \mathbf{q}_d, \mathbf{q}_{12})$ in eq. (4) by exchanging $p_a \leftrightarrow p_b$.

3 a_0 cross-section and non-resonant background in the reaction $pp \to dK^+\bar{K}^0$

3.1 a_0-resonance contribution

To illustrate the hierarchy of the different mechanisms in the case of a_0 production we present in fig. 3 our results for the total cross-section of the reaction $pp \to da_0^+$. As in ref. [28] the a_0NN coupling constant was taken from the Bonn model [37]. For the virtual nucleon we used the standard form factor given by eq. (41) in the appendix with a cut-off parameter $\Lambda_N = 1.3\,\mathrm{GeV}$, which satisfies the constraints found in our recent analysis of the $\pi N \to NK\bar{K}$ and $NN \to NNK\bar{K}$ reactions [30] (see comment after eq. (41)). Moreover, using this approach we can simultaneously describe the LBL data on the forward differential cross-section of the reaction $pp \to da_0^+$ at $3.8\,\mathrm{GeV}/c$ [31]. In practical terms: the cut-off parameter Λ_N may also be defined by normalizing the u-channel contribution to the LBL data.

The parameters of the Regge model have been fixed by Achasov and Shestakov [14] in fitting Brookhaven data on the reaction $\pi^- p \to a_0^0 n$ at $19\,\mathrm{GeV}/c$ [38]. All other parameters were taken the same as in ref. [30] (see also the appendix). As seen in fig. 3, the dominant contribution to the cross-section of the reaction $pp \to da_0^+$ near threshold comes from the u-channel mechanism (shown by the bold dashed line) and all other contributions from f_1- and η-meson exchanges, s-channel nucleon exchange and b_1- and ρ_2-Reggeons can be neglected (for the forward differential cross-section this result was obtained earlier in ref. [28]).

The a_0-resonance contribution to the cross-section of the reaction $pp \to dK^+\bar{K}^0$ is calculated by convoluting

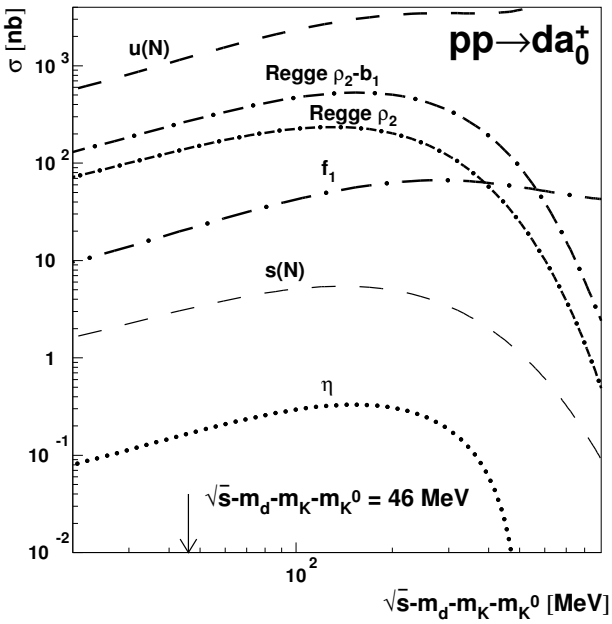

Fig. 3. Total cross-section of the $pp \to da_0^+$ reaction as a function of the c.m. excess energy. The contributions of the u- and s-channel exchanges are shown by the bold dashed and thin dashed lines, respectively. The lower long-dash-dotted line and the dotted line describe the f_1- and η-exchanges. The dash-dotted line stands for the combined ρ_2- and b_1-Reggeon exchanges, while the model result for the single ρ_2-Reggeon exchange is shown by the short-dash-dotted line. The arrow indicates the the excess energy $Q = 46\,\mathrm{MeV}$ of the ANKE experiment.

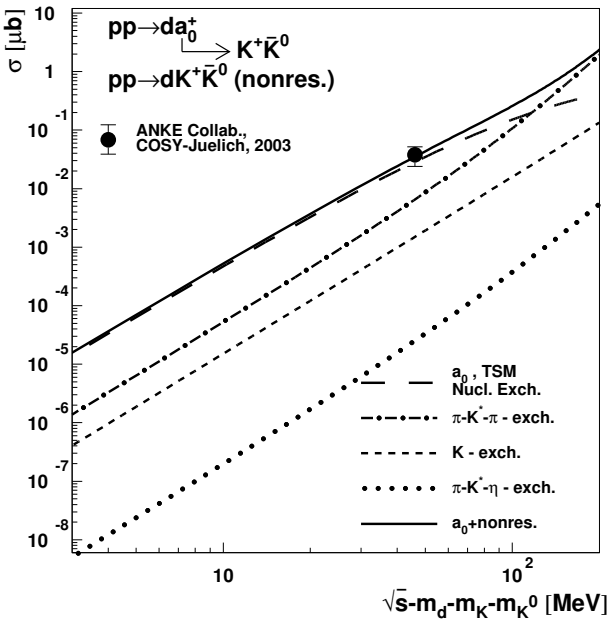

Fig. 4. Total cross-section of the $pp \to dK^+\bar{K}^0$ reaction as a function of the c.m. excess energy. The a_0-resonance part of the cross-section is displayed by the long-dashed line. The dash-dotted and dotted lines show the background corresponding to $\pi - K^\star - \pi$- and $\pi - K^\star - \eta$-exchange mechanisms, respectively. The K-exchange contribution is shown by the short-dashed line. The solid line displays the sum of all contributions. The bold point shows the experimental cross-section from ref. [26].

the cross-section of the a_0^+ production with the Flatté mass distribution (see eq. (8) and also ref. [30]). The result for the dominant a_0-resonance part corresponding to the diagram in fig. 1a) is shown by the long-dashed line in fig. 4. The parameters of the Flatté mass distribution are taken from ref. [34]: $m_0 = 999\,\mathrm{MeV}$, $g_{\pi\eta} = 324\,\mathrm{MeV}$ and $g^2_{K\bar{K}}/g^2_{\pi\eta} = 1.03$. As follows from fig. 3, the total cross-section of the reaction $pp \to da_0^+$ at $p_{\mathrm{lab}} = 3.46\,\mathrm{GeV}$ ($Q = 46\,\mathrm{MeV}$) in the narrow a_0 width limit is about $1.2\,\mu$b. After convolution with the Flatté distribution we find that $\sigma(pp \to da_0^+ \to K^+\bar{K}^0)$ is about 28 nb (see fig. 4). The effective branching ratio for the a_0 decay to the $K\bar{K}$ mode is 0.023 at $Q = 46\,\mathrm{MeV}$. Such a large suppression as compared with the standard value $\Gamma_{K\bar{K}}/\Gamma_{\pi\eta} = 0.177 \pm 0.024$ [39] is related to the phase space limitation and the P-wave character of a_0 production in the reaction $pp \to da_0^+$ near threshold.

3.2 Background contributions

An important problem is to understand the role of the non-resonant contribution to the $pp \to dK^+\bar{K}^0$ cross-section. In ref. [30] the $\pi - K^\star - \pi(\eta)$-exchange mechanisms for non-resonant $K\bar{K}$ production in the reactions $\pi N \to NK\bar{K}$ and $NN \to NNK\bar{K}$ has been considered. The results of calculations for the $\pi N \to NK\bar{K}$ cross-sections in different isospin channels showed that the a_0-resonant part is expected to be more pronounced at $Q \leq 250\,\mathrm{MeV}$ while the non-resonant background might become dominant at $Q \geq 250\,\mathrm{MeV}$ (see fig. 4 in ref. [30]). The analysis of different isospin channels of the reaction $NN \to NNK\bar{K}$ demonstrated that the production of the a_0 —as compared to the background— is more pronounced in the reaction $pp \to pnK^+\bar{K}^0$ than in the reaction $pp \to ppK^+K^-$.

Here we use these previous results to analyze the role of the non-resonant background in the $pp \to dK^+\bar{K}^0$ reaction. The diagrams describing $\pi - K^\star - \pi(\eta)$- and K-exchange mechanisms are shown in fig. 2a) and b), respectively. The results of the calculations are presented in fig. 4. The dash-dotted and dotted lines in fig. 4 display the background corresponding to $\pi - K^\star - \pi$- and $\pi - K^\star - \eta$-exchange mechanisms, respectively, while the K-exchange contribution is shown by the short-dashed line. It can be seen from fig. 4 that this contribution is much smaller than the cross-section for the $\pi - K^\star - \pi$-exchange and may safely be neglected.

As follows from the G-parity constraints (see comment after eq. (15)) the $\pi - K^\star - \pi$-mechanism contributes mainly to the P-wave in the $K^+\bar{K}^0$-system, while the $\pi - K^\star - \eta$-mechanism contributes dominantly to the S-wave. The latter, in principle, via $K\bar{K}$-FSI can contribute to the resonant a_0 channel where the kaons are also produced in a relative S-wave. However, we neglect this in the following, since the contribution from this channel is

very small (see dotted line in fig. 4) and conclude that $K\bar{K}$ pairs from background will predominantly be in a P-wave, while in the case of a_0 decay it will be produced in the S-wave (see also sect. 2 and ref. [30]). According to the long-dashed line in fig. 4, the resonant part is dominant up to $Q \simeq 100\,\mathrm{MeV}$. The background is seen to give an important contribution only for $Q \geq 100\,\mathrm{MeV}$.

As mentioned before, the TSM gives an integrated cross-section of about 28 nb at $Q = 46\,\mathrm{MeV}$ for the a_0-resonance part. As concerning the contribution of the P-wave $K\bar{K}$ pairs, we normalized it here to 6.5 nb at the same Q. This value was obtained in ref. [26] from the best fit to the data. To describe it within the $\pi - K^\star - \pi$-exchange model we use the cut-off parameter $\Lambda_{K^\star}(K^\star\pi K) = 1.25\,\mathrm{GeV}$. Using eqs. (2), (4), (6) and (14)-(15), one can find that the leading term for the $K\bar{K}$ P-wave part of the $pp \to dK^+\bar{K^0}$ amplitude has the following spin structure:

$$T^{\pi-K^\star-\pi}_{pp\to dK^+\bar{K^0}} \sim \varphi^T_{\lambda_a}(\mathbf{p}_a)\ (-i\sigma_2)(\boldsymbol{\sigma}\cdot\mathbf{p}_a)(\boldsymbol{\sigma}\cdot\boldsymbol{\epsilon}^{*(d)}) \times(\boldsymbol{\sigma}\cdot\mathbf{p}_a)(\mathbf{p}_a\cdot\mathbf{q}_{12})\ \varphi_{\lambda_b}(\mathbf{p}_b). \quad (19)$$

Therefore, within the $\pi - K^\star - \pi$-exchange model the background has the following angular distribution:

$$\frac{\mathrm{d}\sigma}{\mathrm{d}\Omega_{12}} \simeq N\cos^2\theta_{12}\,, \quad (20)$$

where $d\Omega_{12} = d\cos\theta_{12}\ d\varphi_{12}$, with Ω_{12} being the solid angle for the $K\bar{K}$ relative momentum $\mathbf{q}_{12}$. The angular distribution in θ_{12} as given by eq. (20) is in good agreement with the experimental data [26]. However, the TSM does not describe the distribution on the deuteron scattering angle: it predicts a forward peak [28] instead of a forward dip found in the ANKE experiment (see fig. 4 in ref. [26]). A possible solution of this discrepancy is presented in the next section within the Quark-Gluon Strings Model (QGSM).

4 The reaction NN → da$_0$ in the QGSM

As we have argued in the previous section, the model based on the effective Lagrangian approach can describe the energy behaviour of the total cross-section of the reaction $NN \to da_0$. However, it fails to reproduce the angular dependence of the differential cross-section. Remarkably, even at threshold the typical values of the momentum transfer in the reaction $NN \to da_0$ exceed $1\,\mathrm{GeV}^2$. Thus, a complete description of this reaction would require to take into account relativistic effects as well as quark degrees of freedom. This can be done, for example, within the framework of the Quark-Gluon Strings Model (QGSM), which recently has successfully been applied in refs. [40–42] to the description of deuteron photodisintegration at energies above 1 GeV at all angles.

This model —proposed originally by Kaidalov [43, 44]— is based on two ingredients: i) a topological expansion in QCD, and ii) a space-time picture of the interactions between hadrons that takes into account the confinement of quarks. In a more general sense, the QGSM can be considered as a microscopic (non-perturbative) model of Regge phenomenology for the analysis of exclusive and inclusive hadron-hadron and photon-hadron reactions on the quark level. The main assumption of the QGSM is that the amplitudes $T(\gamma d \to pn)$ and $T(NN \to a_0 d)$ can be described by planar graphs with three valence-quark exchange in t(or u)-channels with any number of gluon exchanges between them (fig. 5). This corresponds to the contributions of the t- and u-channel nucleon Regge trajectories. In the space-time picture, the intermediate s-channel consists of a string (or color tube) with q and $5q$ states at the ends.

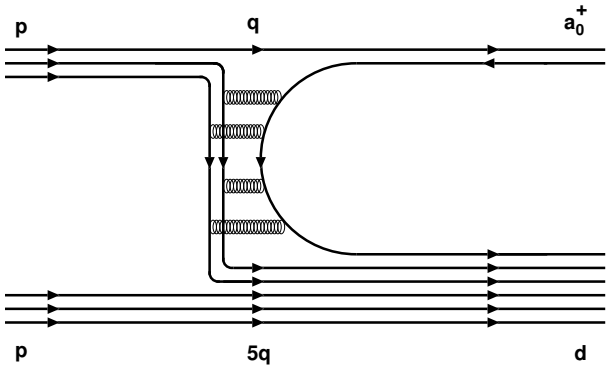

Fig. 5. Planar quark diagram describing the reaction $pp \to a_0^+ d$ in the quark-gluon-strings model (QGSM).

It is interesting to compare the u-channel mechanism of the two-step model described by fig. 1a) with the planar quark diagram of the QGSM shown in fig. 5. If the former describes only one-nucleon exchange in the u-channel, the latter is equivalent to an infinite sum of contributions for all baryon resonances with isospin 1/2 lying on the nucleon Regge trajectory.

4.1 Spin structure of the NN → da$_0$ amplitude in the QGSM

The spin dependence of the $\gamma d \to pn$ amplitude has been evaluated in ref. [40] by assuming that all intermediate quark clusters have minimal spins and the s-channel helicities in the quark-hadron and hadron-quark transition amplitudes are conserved. In this limit, the spin structure of the amplitude $T(\gamma d \to pn)$ can be written as (see ref. [40], comment after eq. (27))

$$\langle p_3,\lambda_p; p_4,\lambda_n|\hat{T}\,(s,t)\,|p_2,\lambda_d; p_1,\lambda_\gamma\rangle \simeq \bar{u}_{\lambda_p}(p_3)\hat{\epsilon}_{\lambda_\gamma} \times[A_{\gamma d\to pn}(s,t)(\hat{p}_3-\hat{p}_1)+B_{\gamma d\to pn}(s,t)m] \times\hat{\epsilon}_{\lambda_d}v_{\lambda_n}(p_4), \quad (21)$$

where m is the nucleon mass, p_1, p_2, p_3, and p_4 are the 4-momenta of the photon, deuteron, proton and neutron, respectively, and λ_i denotes the s channel helicity of the i-th particle. The invariant amplitudes $A_{\gamma d\to pn}(s,t)$ and $B_{\gamma d\to pn}(s,t)$ have similar Regge asymptotics (see below).

It is possible to show (cf. ref. [40]) that at small scattering angles the ratio $R_{\gamma d} = A_{\gamma d\to pn}(s,t)/B_{\gamma d\to pn}(s,t)$ is a smooth function of t and can be considered as an effective constant that depends on the ratio of the nucleon mass to the constituent quark mass m_q: $R \simeq m/(2m_q)$. Such a simple interpretation of R in general does not work at large scattering angles.

It is interesting to note that the spin structure of the $\gamma d \to pn$ amplitude in eq. (21) is very similar to the amplitude within the Reggeized Nucleon Born Term Approach (RNBTA), where $R_{\gamma d} = 1$ is directly related to the spin structure of the nucleon propagator (see refs. [45,46]).

In complete analogy with eq. (21) the spin structure of the amplitude $T(pp \to da_0^+)$ can be written as

$$\langle q_d, \lambda_d; q_{a_0}|\hat{T}\,(s,t)\,|p_a,\lambda_a;p_b,\lambda_b\rangle \simeq \bar{v}_{\lambda_a}(p_a)\hat{\epsilon}^*_{\lambda_d} \times \left[A_{pp\to da_0^+}(s,t)(\hat{p}_a - \hat{q}_{a_0}) + B_{pp\to da_0^+}(s,t)m\right] \times \hat{u}_{\lambda_b}(p_b). \quad (22)$$

In order to achieve consistency of the differential cross-section $\mathrm{d}\sigma/\mathrm{d}t$ with the Regge behaviour, we use the following parametrization of the amplitude $B_{pp\to da_0^+}(s,t)$:

$$\left|B_{pp\to da_0^+}(s,t)\right|^2 = \frac{1}{s}\ \left|\mathcal{M}_{\mathrm{Regge}}(s,t)\right|^2, \quad (23)$$

where

$$\mathcal{M}_{\mathrm{Regge}}(s,t) = F(t)\left(\frac{s}{s_0}\right)^{\alpha_N(t)} \times \exp\left[-i\ \frac{\pi}{2}\left(\alpha_N(t) - \frac{1}{2}\right)\right]. \quad (24)$$

Here $\alpha_N(t)$ is the trajectory of the nucleon Regge pole and $s_0 = 4\,\mathrm{GeV}^2 \simeq m_d^2$. We take the dependence of the residue $F(t)$ on t in the form

$$F(t) = B_{\mathrm{res}}\left[\frac{1}{m^2 - t}\ \exp\left(R_1^2 t\right) + C\ \exp\left(R_2^2 t\right)\right], \quad (25)$$

as used previously in refs. [47,48] for the description of the reactions $pp \to d\pi^+$ and $\bar{p}d \to p\pi^-$ at $-t \le 1.6\,\mathrm{GeV}^2$ as well as for the analysis of deuteron photodisintegration at $E_\gamma \ge 1\,\mathrm{GeV}$ (see ref. [40]). In eq. (25) the first term in the square brackets contains the nucleon pole and the second term accounts for the contribution of non-nucleonic degrees of freedom in the deuteron.

The amplitudes defined by eqs. (21) and (22) have a rather simple covariant structure and can be extrapolated to large angles. As shown in ref. [40], the energy behavior of the cross-section for the reaction $\gamma d \to pn$ at large angles crucially depends on the form of the Regge trajectory $\alpha_N(t)$ for large negative t. Best agreement with experimental data is obtained for a logarithmic form:

$$\alpha_N(t) = \alpha_N(0) - (\gamma\nu)\ln(1 - t/T_B), \quad (26)$$

where the intercept $\alpha_N(0) = -0.5$, the slope $\alpha'_N(0) = 0.8$–$0.9\,\mathrm{GeV}^{-2}$ and $T_B = 1.5$–$1.7\,\mathrm{GeV}^2$. We adopt the following values for the parameters of the residue $F(t)$ of eq. (25):

$$C = 0.7\,\mathrm{GeV}^{-2},\ R_1^2 = 1\text{–}2\,\mathrm{GeV}^{-2},\ R_2^2 = 0.03\,\mathrm{GeV}^{-2}.$$

These parameters of the residue and trajectory, except for the overall normalization factor B_{res}, are not very different from those determined by fitting data on the reactions $pp \to d\pi^+$ at $-t \le 1.6\,\mathrm{GeV}^2$ [47] and $\gamma d \to pn$ at $E_\gamma \ge 1\,\mathrm{GeV}$ [40].

We considered the $pp \to da_0^+$ amplitude (22) within the RNBTA, *i.e.* for a fixed ratio

$$R_{a_0 d} = A_{pp\to da_0^+}(s,t)/B_{pp\to da_0^+}(s,t) = 1,$$

as well as its generalization corresponding to the QGSM. The spin structure of the amplitude within the QGSM takes into account quark degrees of freedom and the parameter $R_{a_0 d}$ may be different from 1. In line with ref. [28], we also treat the ratio $R_{a_0 d}$ as a free parameter. The parameters of the residue, trajectory and the ratio $R_{a_0 d}$ used for our calculations are given in tables 1 and 2.

Table 1. Parameters of the Regge trajectory (26) and the residue (25) for the reactions $\gamma d \to pn$ (Set(γd)) and $pp \to da_0^+$ (Set($a_0 d$)).

Parameter	Set(γd) [40]	Set($a_0 d$)
$\alpha'_N(0)$ (GeV^{-2})	0.9	0.8
T_B (GeV^2)	1.7	1.5
R_1^2 (GeV^{-2})	2	1

Table 2. Parameters of the trajectory and residue, normalization factor B_{res} and the ratio $R_{a_0 d}$ used for the $pp \to da_0^+$ amplitude calculation within the RNBTA and QGSM.

Parameters	RNBTA	QGSM	
Trajectory & residue	Set(γd)	Set(γd)	Set($a_0 d$)
B_{res} ($\mathrm{nb}^{1/2}\cdot\mathrm{GeV}^3$)	5.23×10^3	3.19×10^3	2.67×10^3
$R_{a_0 d}$	1	-4	-4

4.2 Numerical results

In fig. 6 we show the a_0-resonance contribution to the $pp \to dK^+\bar{K}^0$ cross-section calculated within the QGSM (dashed curve) as well as the prediction of the TSM (long-dashed line). The dash-dotted line displays the background corresponding to the $\pi - K^\star - \pi$-exchange mechanism. Since we have $K\bar{K}$ pairs in a relative S-wave basically due to direct a_0-resonance production, we have normalized the results of the QGSM at $Q = 46\,\mathrm{MeV}$ to the experimental value 31.5 nb, which was found for the $K\bar{K}$ S-wave part [26]. The corresponding values of the normalization factor B_{res} are given in table 2. In fig. 6 we display the result of the QGSM with parameters of Set ($a_0 d$). Since the calculations with Set(γd) give practically the same answer, we discard an explicit representation in this figure. As seen from fig. 6, the energy dependence of the a_0-resonance contribution of the cross-section predicted

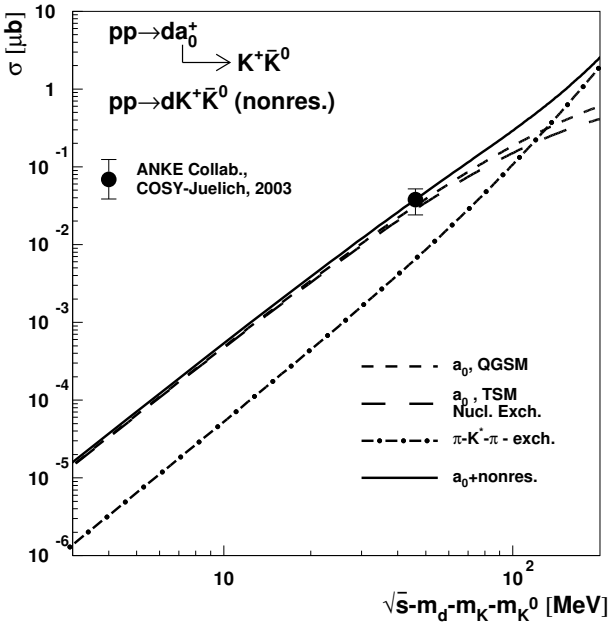

Fig. 6. Total cross-section of the $pp \to dK^+\bar{K}^0$ reaction as a function of the c.m. excess energy. The long-dashed line displays the a_0-resonance part of the cross-section calculated within the TSM (same as in fig. (4)), which is very close to the results for the a_0 contribution from the QGSM (short-dashed line). The dash-dotted line shows the background corresponding to the $\pi - K^\star - \pi$-exchange mechanism, while the solid line displays the sum of the background and the a_0 production cross-section calculated within the QGSM. The full dot shows the experimental cross-section from ref. [26].

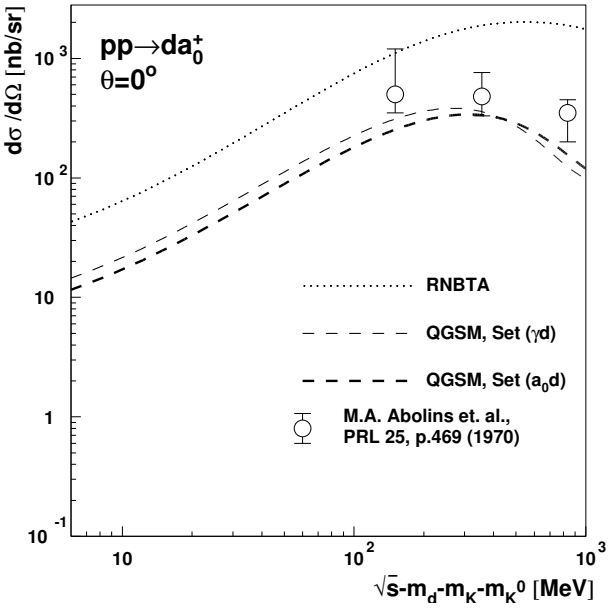

Fig. 7. Forward differential cross-section of the reaction $pp \to da_0^+$ as a function of the c.m. excess energy. The open dots are the experimental data from ref. [31]. The dotted line shows the prediction of the RNBTA. The thin and thick dashed curves display the results of the QGSM with parameters of Set(γd) and Set($a_0 d$), respectively.

by the TSM and QGSM is very similar at $Q \leq 200\,\mathrm{MeV}$. The solid line in fig. 6 displays the sum of the a_0-resonance production cross-section calculated within the QGSM and the $K\bar{K}$ P-wave background contribution.

In order to check the consistency of our model for a_0 production in the $pp \to da_0^+$ reaction, we compare the calculated forward differential cross-section with the LBL data [31] in fig. 7. The dotted line shows the prediction of the RNBTA. The calculations within the QGSM —normalized to the ANKE data on the reaction $pp \to da_0^+ \to K^+\bar{K}^0$— are in a good agreement with the differential cross-sections measured at LBL [31] (open circles).

The calculated angular and invariant mass distributions for the $pp \to dK^+\bar{K}^0$ reaction at $Q = 46\,\mathrm{MeV}$ are shown in fig. 8 in comparison with the experimental data [26]. The dashed lines correspond to $K^+\bar{K}^0$ production through the a_0-resonance and have been calculated within the QGSM using the parameters from Set($a_0 d$). The dash-dotted lines describe the $K\bar{K}$ P-wave background calculated within the $\pi - K^\star - \pi$-exchange model. The solid lines indicate the sum of the a_0-resonance and background contributions. In the upper part of the figure we show also the angular distribution for deuterons calculated in the QGSM with parameters of Set(γd). The almost isotropic angular dependence given by this version of the QGSM (thin solid line) is in a reasonable agreement with the data. The angular distribution of deuterons for the a_0 contribution as calculated within the RNBTA is presented by the dotted line and gives a sharp forward peak similarly to the non-relativistic two-step model [28]. Therefore, both models —TSM and RNBTA— are not able to reproduce the experimental deuteron angular distribution [26]. The best description of the data (bold solid line) is obtained by the QGSM with parameters of the Set ($a_0 d$).

Therefore, the QGSM gives a rather good description of the ANKE data on the reaction $pp \to dK^+\bar{K}^0$ at $Q = 46\,\mathrm{MeV}$ [26] and, simultaneously, is in agreement with the forward differential cross-section of the reaction $pp \to da_0^+$ measured at LBL at 3.8, 4.5 and 6.3 GeV/c [31].

In fig. 9 we present the predictions for the angular and mass distributions at $Q = 107\,\mathrm{MeV}$, where corresponding experimental data from ANKE are expected soon. It is important to note that our model for the $pp \to d\bar{K}^0 K^+$ reaction predicts that the ratio of the background to the a_0 contribution will increase by a factor of 3. Therefore, the background contribution is expected to be about 40% at $Q = 107\,\mathrm{MeV}$. As seen from the lower part of fig. 9, the a_0-resonance part can be separated from the contribution from the $K^+\bar{K}^0$ P-wave background: Most of the events related to the a_0-resonance are concentrated in the lower part of the $K^+\bar{K}^0$ mass spectrum, whereas the main contribution of the background shows up at higher invariant mass.

5 Final-state interactions

As has been stressed in ref. [27], the reaction $pp \to dK^+\bar{K}^0$ might be sensitive to both the $K^+\bar{K}^0$ and $\bar{K}d$

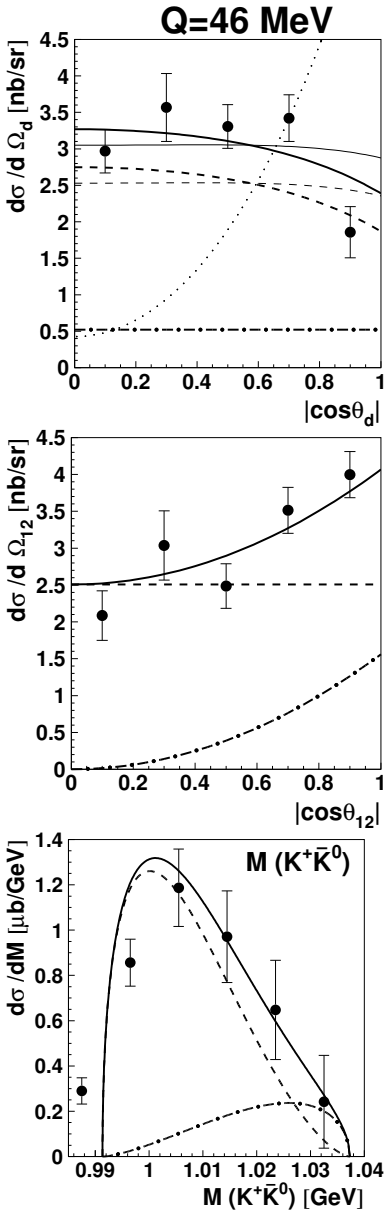

Fig. 8. Angular distributions (upper and middle part) and invariant mass distribution (lower part) for the $pp \to dK^+\bar{K}^0$ reaction at $Q = 46\,\mathrm{MeV}$ in comparison with the data from ref. [26]. The dashed (dash-dotted) line corresponds to $K^+\bar{K}^0$ production in a relative S-(P-) wave and the solid line is the sum of both contributions. The a_0-resonance contribution shown by the thick and thin dashed lines results from the QGSM with parameters of Set($a_0 d$) and Set(γd), respectively. The dotted line is the result from the RNBTA. Θ_d and Θ_{12} are the polar angles for the c.m. deuteron momentum and for the $K\bar{K}$ relative momentum, respectively.

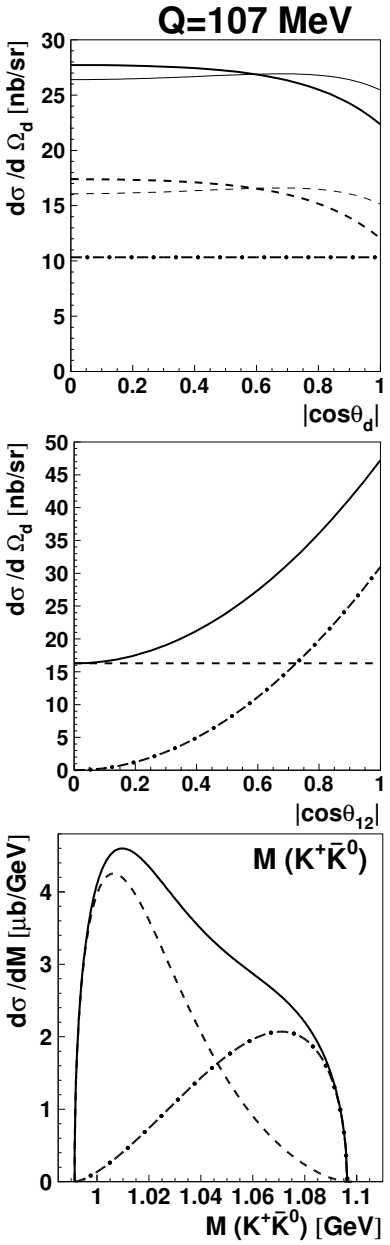

Fig. 9. Angular distributions (upper and middle part) and invariant mass distribution (lower part) for the $pp \to dK^+\bar{K}^0$ reaction at $Q = 107\,\mathrm{MeV}$ (see fig. 8 for the description of the lines.)

final-state interactions (FSI). The interaction of the K^+ with protons and neutrons is rather weak [49] and following ref. [27] we will neglect it. Within our model we can describe the S-wave $K\bar{K}$ cross-section by direct a_0^+ production with subsequent decay $a_0^+ \to K^+\bar{K}^0$. Contributions from non-resonant S-wave $K\bar{K}$ production turned out to be negligibly small, whereas the P-wave $K\bar{K}$ FSI is small due to centrifugal suppression. Thus we only have to consider the $\bar{K}d$ FSI. To estimate the role of the S-wave $\bar{K}d$ FSI, we use the Foldy-Brueckner adiabatic approach based on the multiple scattering (MS) formalism (see ref. [50]). Note that this method has already been used for the calculation of the enhancement factor for the reactions $pd \to {}^3\mathrm{He}\eta$ [51] and $pn \to d\eta$ [32].

In the Foldy-Brueckner adiabatic approach, the $\bar{K}^0 d$ wave function —defined at fixed coordinates of the proton ($\mathbf{r}_p$) and the neutron ($\mathbf{r}_n$) (see ref. [50] for details)—

reads as

$$\Psi_k\big(\mathbf{r}_{\bar{K}^0},\mathbf{r}_p,\mathbf{r}_n\big) = \exp\big(i\mathbf{k}\mathbf{r}_{\bar{K}^0}\big) + \frac{t_{\bar{K}^0p}}{D}\,\frac{\exp\left(ikr_{\bar{K}^0p}\right)}{r_{\bar{K}^0p}} \times\left(\exp\left(i\mathbf{k}\mathbf{r}_p\right) + t_{\bar{K}^0n}\,\frac{\exp\left(ikr_{pn}\right)}{r_{pn}}\exp\left(i\mathbf{k}\mathbf{r}_n\right)\right) + \frac{t_{\bar{K}^0n}}{D}\,\frac{\exp\left(ikr_{\bar{K}^0n}\right)}{r_{\bar{K}^0n}} \times\left(\exp\left(i\mathbf{k}\mathbf{r}_n\right) + t_{\bar{K}^0p}\frac{\exp\left(ikr_{pn}\right)}{r_{pn}}\exp\left(i\mathbf{k}\mathbf{r}_p\right)\right), \quad (27)$$

where

$$D = \left(1 - t_{\bar{K}^0p}t_{\bar{K}^0n}\,\frac{\exp\left(2ikr_{pn}\right)}{r_{pn}^2}\right). \quad (28)$$

Here $\mathbf{r}_{pn} = \mathbf{r}_p - \mathbf{r}_n$, $\mathbf{r}_{\bar{K}^0p} = \mathbf{r}_{\bar{K}^0} - \mathbf{r}_p$, $\mathbf{r}_{\bar{K}^0n} = \mathbf{r}_{\bar{K}^0} - \mathbf{r}_n$ and $\mathbf{k} = \mathbf{q}_{1d}\,\frac{m_d+m_{\bar{K}^0}}{m_d}$ and k,r_{pn}, etc., are the moduli of these vectors; $t_{\bar{K}^0N}$ is the $\bar{K}^0N$ t-matrix which is related to the scattering amplitude $f_{\bar{K}^0N}$ by

$$t_{\bar{K}^0N}(k_{\bar{K}^0N}) = \left(1 + \frac{m_{\bar{K}^0}}{m}\right) f_{\bar{K}^0N}(k_{\bar{K}^0N}). \quad (29)$$

Note that we use the unitarized scattering length approximation for the latter, *i.e.*

$$f^I_{\bar{K}N}(k_{\bar{K}N}) = \Big(\big(a^I_{\bar{K}N}\big)^{-1} - ik_{\bar{K}N}\Big)^{-1}, \quad (30)$$

where $k_{\bar{K}N}$ is the modulus of the relative $\bar{K}N$ momentum and I denotes the isospin of the $\bar{K}N$-system.

The $\bar{K}^0d$ scattering length then is defined as

$$A^{\rm MS}_{\bar{K}^0d} = \frac{m_d}{m_{\bar{K}^0}+m_d} \times\left\langle\frac{t_{\bar{K}^0p}(k_{\bar{K}^0p}=0) + t_{\bar{K}^0n}(k_{\bar{K}^0n}=0) + t_r}{1 - t_{\bar{K}^0p}(k_{\bar{K}^0p}=0)t_{\bar{K}^0n}(k_{\bar{K}^0n}=0)/r^2}\right\rangle, \quad (31)$$

and the FSI enhancement factor as

$$\lambda^{\rm MS}(q_{1d}) = |\langle\Psi_k(\mathbf{r}_{\bar{K}^0}=0,\mathbf{r}_p=\mathbf{r}/2,\mathbf{r}_n=-\mathbf{r}/2)\rangle|^2. \quad (32)$$

In eq. (31) we have used the abbreviation

$$t_r = \frac{2t_{\bar{K}^0p}(k_{\bar{K}^0p}=0)t_{\bar{K}^0n}(k_{\bar{K}^0n}=0)}{r}. \quad (33)$$

To describe the deuteron structure we use the Paris wave function [52]. The $\bar{K}N$ scattering lengths $a^0_{\bar{K}N}$ and $a^1_{\bar{K}N}$ are taken from ref. [53]:

i) $a_0 = -1.57 + i\,0.78\,\text{fm}$, $a_1 = 0.32 + i\,0.75\,\text{fm}$ (CSL set);

ii) $a_0 = -1.59 + i\,0.76\,\text{fm}$, $a_1 = 0.26 + i\,0.57\,\text{fm}$ (K-matrix set).

We recall that the $\bar{K}N$ scattering length is strongly repulsive for the isospin channel $I = 0$ and moderately attractive for $I = 1$. In the single scattering approximation then a slight repulsion adds up for the $\bar{K}d$-system

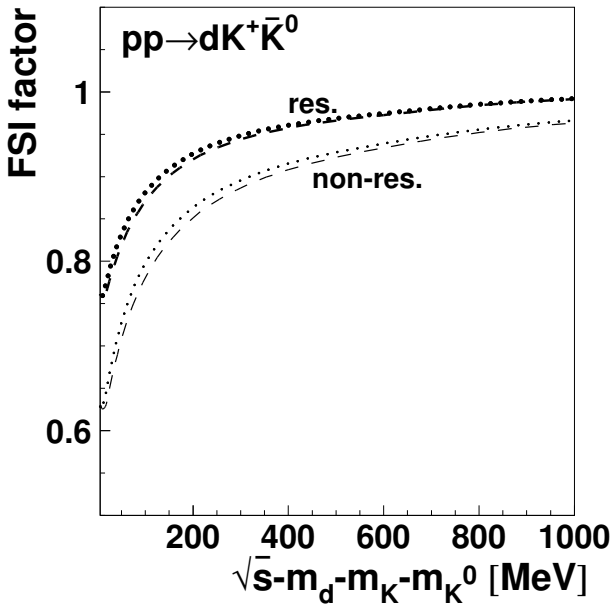

Fig. 10. The final-state interaction factor for the reaction $pp \to dK^+\bar{K}^0$ as a function of the energy above threshold. The upper and lower lines correspond to a_0 production and the $K\bar{K}$ background, respectively. The dashed and dotted lines correspond to the CSL and K-matrix sets of the $\bar{K}N$ scattering length [53], respectively.

$A^{IA}_{\bar{K}d} = -0.39 + i\ 1.72\,\text{fm}$ [53]. Results from Faddeev calculations with separable $\bar{K}N$ potentials —as carried out in ref. [54]— give $A_{\bar{K}d} = -1.34 + i\ 1.04\,\text{fm}$, *i.e.*, they predict a larger $\bar{K}d$ repulsion. We remind the reader that a repulsion in the low-energy $\bar{K}d$-system can lead to a FSI suppression factor (< 1); on the other hand, any attraction leads to a FSI enhancement factor (> 1).

Evidently, the FSI effect is most important close to threshold and is due to the long-range coherent S-wave $\bar{K}d$ interaction. Therefore, one can safely assume that the range of the FSI is much larger than the range of the "hard" interaction, which is responsible for the production of the $K\bar{K}$-meson pair. In this case, the basic production amplitude and the FSI can be factorized [50], *i.e.* the FSI can be taken into account by multiplying the production cross-section by the FSI factor.

The partial wave structure of the final state for the basic production amplitude corresponds to $[(\bar{K}^0K^+)_sd]_P$, for a_0 production, and to $[(\bar{K}^0K^+)_pd]_S$ for the $K\bar{K}$ background. To calculate the corresponding FSI factors we expressed these partial waves in terms of partial amplitudes of the second basis with $[(d\bar{K}^0)_sK^+]_P$ and $[(d\bar{K}^0)_pK^+]_S$. Then we have to take into account that only the first term of the second basis is renormalized due to the S-wave $\bar{K}d$ interaction (see, *e.g.*, ref. [27]). According to experimental data [26], the latter configuration gives about 50% contribution to the total production cross-section of the reaction $pp \to dK^+\bar{K}^0$ at $Q = 46\,\text{MeV}$ [55].

The results of our calculations for the FSI effect on the cross-section of the reaction $pp \to dK^+\bar{K}^0$ as well as on the $K^+\bar{K}^0$ and $d\bar{K}^0$ mass distributions are shown in

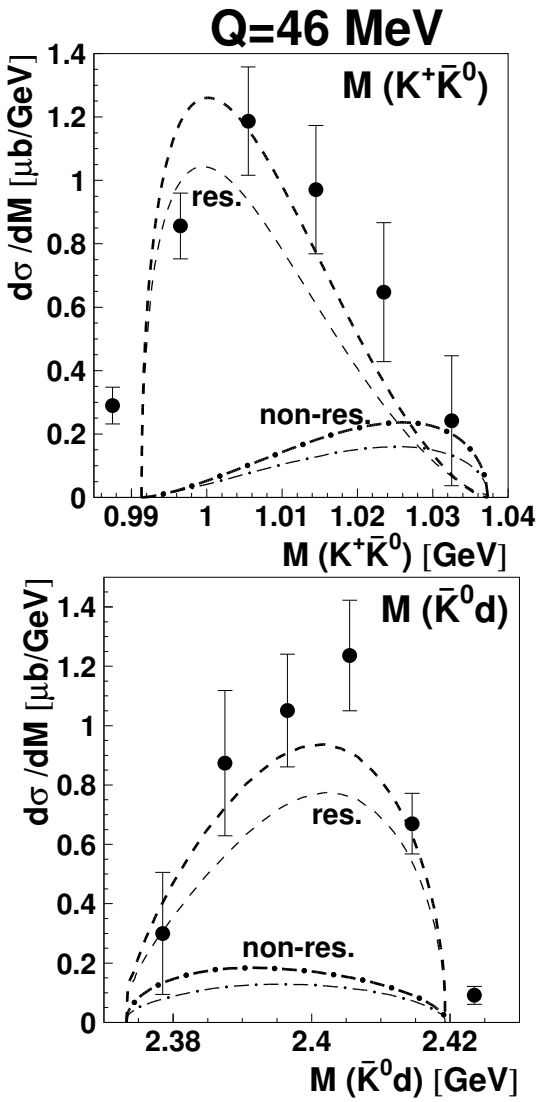

Fig. 11. Invariant mass distributions for the $K^+\bar{K}^0$ (upper part) and $d\bar{K}^0$ (lower part) systems for the reaction $pp \to dK^+\bar{K}^0$ at $Q = 46\,\mathrm{MeV}$. The dashed (dash-dotted) lines are calculated for the resonance (non-resonance) contributions. The thick (thin) curves describe the contributions without (with) the FSI included. The experimental data are taken from ref. [26].

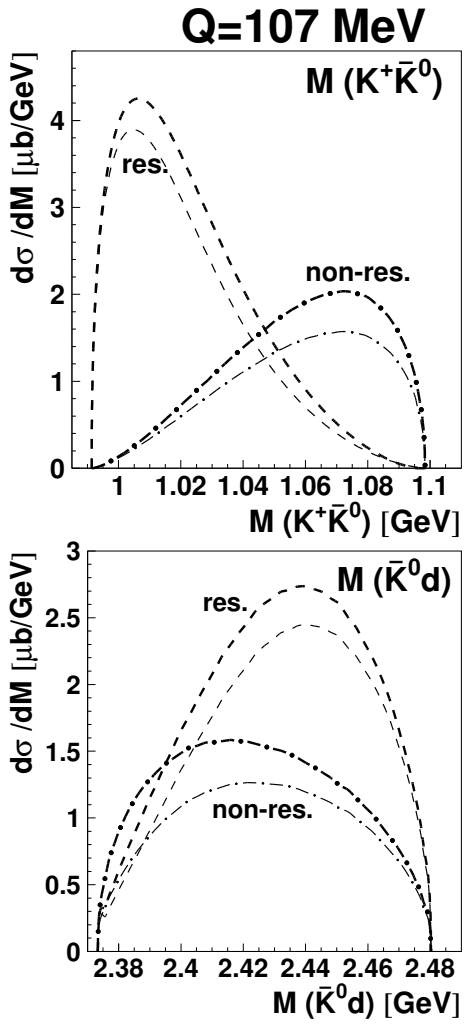

Fig. 12. Invariant mass distributions for the $K^+\bar{K}^0$ (upper part) and $d\bar{K}^0$ (lower part) systems for the reaction $pp \to dK^+\bar{K}^0$ at $Q = 107\,\mathrm{MeV}$. The assignment of the individual lines is the same as in fig. 11.

figs. 10, 11 and 12. We start with the energy dependence of the FSI factor which is presented in fig. 10. The upper and lower lines correspond to a_0 production and the $K\bar{K}$ background, respectively. We find that the FSI factors are smaller than one, as expected from the repulsion in the system (see the discussion above). Furthermore, the suppression of the non-resonant background is larger than for the a_0-resonant channel. In the latter case, the suppression is about 0.81 at $Q = 46\,\mathrm{MeV}$ and 0.88 at 107 MeV, while the background is suppressed by 0.7 at $Q = 46\,\mathrm{MeV}$ and 0.79 at 107 MeV, respectively. The dashed and dotted lines correspond to the CSL and K-matrix sets of the $\bar{K}N$ scattering length [53]; both parameter-sets lead to approximately the same suppression factors.

The invariant mass distributions for the $K^+\bar{K}^0$ and $d\bar{K}^0$ systems are shown in figs. 11 and 12 for $Q = 46\,\mathrm{MeV}$ and 107 MeV, respectively. The dashed (upper) lines are calculated for the resonance contributions, while the dash-dotted (lower) lines stand for the non-resonance contributions. The bold lines describe the contributions calculated without FSI, where the thin lines with FSI are always slightly lower in line with fig. 10.

We note that the QGSM cannot predict the absolute value of the cross-section and has been "normalized" to the data at 46 MeV. If we rescale the respective mass distribution up by ~ 20 %, we obtain distributions practically identical to the bold dashed lines calculated without FSI. Therefore, increasing the normalization of the QGSM by 1.2 our calculations for the $K^+\bar{K}^0$ and $d\bar{K}^0$ mass distributions will be again in a good agreement with the ANKE data [26]. Let us note that the predictions of ref. [27] on strong distorsions of the $K^+\bar{K}^0$ and $\bar{K}^0 d$ invariant mass

spectra by the $\bar{K^0}d$ FSI were not confirmed by the experiment [26].

We finally address the validity of the FSI model employed here. The multiple scattering (or fixed center) approach (MSA) was applied to the calculations of the K^-d scattering length in ref. [53] before and has also been compared to full multichannel Faddeev calculations in ref. [56]. In the latter studies it was found that the MSA —with a single-channel absorptive $\bar{K}N$ interaction— gives quite reliable estimates for the real and imaginary parts of the K^-d scattering length. Our results for the latter are in reasonable agreement with the calculation of ref. [53]: we found $A_{\bar{K}d} = -0.78 + i\ 1.23\,\mathrm{fm}$ for the K-matrix set while ref. [53] gives $A_{\bar{K}d} = -0.72 + i\ 0.94\,\mathrm{fm}$ which has to be multiplied additionally by the "reduced mass" factor (see, *e.g.*, [51]):

$$\frac{(1 + m_{\bar{K^0}}/m)}{(1 + m_{\bar{K^0}}/m_d)} \simeq 1.18. \tag{34}$$

This gives $A^*_{\bar{K}d} = -0.85 + i\ 1.11\,\mathrm{fm}$. The agreement with our result is evidently quite good.

6 Conclusions

In this work we have performed a detailed study of a_0 production in the reaction $NN \to dK^+\bar{K}^0$ near threshold and at medium energies. Using the two-step model (TSM) based on an effective Lagrangian approach with one-pion exchange in the intermediate state we have analyzed different contributions to the cross-section of the reaction $NN \to da_0$ corresponding to t-channel diagrams with η- and $f_1(1285)$-meson exchanges as well as s- and u-channel graphs with an intermediate nucleon. We have also considered the t-channel Reggeon mechanism with b_1- and ρ_2-exchanges with parameters normalized to the Brookhaven data for $\pi^-p \to a_0^0 n$ at $18\,\mathrm{GeV}/c$ [38]. These results have been used to calculate the contribution of a_0-mesons to the cross-section of the reaction $pp \to dK^+\bar{K}^0$. We found that the dominant contribution is given by the nucleon u-channel mechanism.

Within this approach, which is practically equivalent to a direct normalization of the u-channel contribution to the LBL data [31] on the forward differential cross-section of the reaction $pp \to da_0^+$ at $3.8\,\mathrm{GeV}/c$, we could reproduce fairly well the total cross-section of the reaction $pp \to dK^+\bar{K}^0$ at $3.46\,\mathrm{GeV}/c$ ($Q = 46\,\mathrm{MeV}$) as measured at COSY [26]. However, the TSM fails to reproduce the experimental distribution in the deuteron scattering angle.

As an alternative and more general approach, we have employed the Quark-Gluon Strings Model (QGSM), that recently has successfully been applied to the description of deuteron photodisintegration data [40,42]. Within the QGSM, there is an almost complete analogy between the amplitudes of the reactions $\gamma d \to pn$ and $NN \to da_0$ because both are described by planar graphs with three valence-quark exchange in the t(or u)-channels (cf. fig. 5). Normalizing the QGSM predictions to the total cross-section of the reaction $pp \to da_0^+ \to dK^+\bar{K}^0$ at $Q = 46\,\mathrm{MeV}$, we have calculated the energy dependence of the cross-section as well as the angular and mass distributions at $Q = 46$ and $107\,\mathrm{MeV}$. The QGSM reproduces the differential experimental distributions at $Q = 46\,\mathrm{MeV}$. We have, furthermore, demonstrated that the QGSM gives also a rather good description of the LBL data at intermediate energies. In order to test the QGSM and its implications, we have made detailed predictions for an excess energy of $107\,\mathrm{MeV}$ that can be controlled experimentally in the near future.

We also analyzed the non-resonant $K\bar{K}$-pair production using a model with $\pi - K^\star - \pi(\eta)$- and K-exchange mechanisms. It is found that the K-exchange mechanism can be neglected. As following from G-parity conservation arguments the $\pi - K^\star - \pi$-mechanism contributes mainly to the P-wave in the $K^+\bar{K}^0$-system, while the $\pi - K^\star - \eta$-mechanism contributes dominantly to the S-wave. The latter channel turned out to be negligibly small. In addition, we have explored the effects from final-state interactions (FSI) in these reactions for the resonant and non-resonant channels. Due to an effective repulsive interaction in the $\bar{K}d$-system the FSI factor turns out to be smaller than one. However, the net suppression found is only in the order of 20% for the a_0 channel, while the background is suppressed by up to $\sim 30\%$. Moreover, the shape of the invariant mass distributions in the $K^+\bar{K}^0$ and $\bar{K}^0d$ channels is practically not influenced by the FSI.

In summary, we conclude that the reaction $pp \to dK^+\bar{K}^0$ at excess energies $Q \leq 100\,\mathrm{MeV}$ should be dominated by the intermediate production of the $a_0(980)$-resonance. For $Q \geq 100\,\mathrm{MeV}$, the non-resonant $K^+\bar{K}^0$-pair production can be important; however, this background gives a dominant contribution to the $K^+\bar{K}^0$ P-wave at higher $K^+\bar{K}^0$ invariant mass. This implies that the experimental program on the study of near-threshold a_0 and f_0 production in pp, pn, pd and dd interactions at COSY-Jülich [21,22] is promising, since the a_0 signal in the $K\bar{K}$ mode can reliably be separated from the non-resonant $K\bar{K}$ background.

Appendix A

In this appendix we present the $\pi N \to N a_0$ amplitudes which were used in sect. 3 for the calculation of the resonant contribution to the reaction $pp \to dK^+\bar{K}^0$.

The t-channel $f_1(1285)$- and η-exchanges are described by the expressions

$$M^t_\eta(\pi^- p \to a_0^- p) = g_{\eta\pi a_0} g_{\eta NN}\ \bar{u}(p_2')\gamma_5 u(p_2) \times \frac{1}{t - m_\eta^2}\ F_{\eta\pi a_0}(t) F_{\eta NN}(t), \tag{35}$$

$$M^t_{f_1}(\pi^- p \to a_0^- p) = g_{f_1\pi a_0} g_{f_1 NN} \times (p_1 + p_1')_\mu \left(g_{\mu\nu} - \frac{q_\mu q_\nu}{m_{f_1}^2}\right) \bar{u}(p_2')\gamma_\nu\gamma_5 u(p_2) \times \frac{1}{t - m_{f_1}^2}\ F_{f_1\pi a_0}(t)\ F_{f_1 NN}(t). \tag{36}$$

Here p_1 and p_1' are the four momenta of π^- and a_0^-, whereas p_2 and p_2' are the four momenta of the initial and final protons, respectively, and $q = p_2' - p_2$, $t = (p_2' - p_2)^2$. The form factors $F_j(t)$ at the different vertices j ($j = f_1NN, \eta NN$) are taken in the form (7).

In the case of η-exchange, we use $g_{\eta NN} = 6.1$, $\Lambda_{\eta NN} = 1.5\,\mathrm{GeV}$ from [37] and $g_{\eta\pi a_0} = 2.2\,\mathrm{GeV}$ (see [30]). The contribution of the f_1-exchange is calculated using $g_{f_1NN} = 14.6$, $\Lambda_{f_1NN} = 2\,\mathrm{GeV}$ from [57] and $g_{f_1a_0\pi} = 2.5$. The latter value for $g_{f_1a_0\pi}$ corresponds to $\Gamma(f_1 \to a_0\pi) = 24\,\mathrm{MeV}$ and $\mathrm{Br}(f_1 \to a_0\pi) = 34\%$ (see ref. [39]). Equation (35) as well as eq. (36) can be represented in the form (13), with the invariant amplitudes $A(s,t)$ and $B(s,t)$ given by

$$A^{\{\eta\}}(s,t) = -g_{\eta\pi a_0} g_{\eta NN}\ \frac{F_{\eta\pi a_0}(t) F_{\eta NN}(t)}{t - m_\eta^2}\,,$$
$$B^{\{\eta\}}(s,t) = 0 \qquad (37)$$

for the η-exchange contribution, and

$$A^{\{f_1\}}(s,t,u) = 2m_N\ \frac{s + t + u - 2(m_{a_0}^2 + m_N^2)}{m_{f_1}^2}$$
$$\times g_{f_1\pi a_0} g_{f_1NN}\ \frac{F_{f_1\pi a_0}(t) F_{f_1NN}(t)}{t - m_{f_1}^2}\,,$$
$$B^{\{f_1\}}(s,t) = 2\ g_{f_1\pi a_0} g_{f_1NN}\ \frac{F_{f_1\pi a_0}(t) F_{f_1NN}(t)}{t - m_{f_1}^2} \qquad (38)$$

for the f_1-exchange.

The amplitudes of the s- and u-channel contributions are defined by the standard expressions

$$M_N^s(\pi^- p \to a_0^0 n) = -\sqrt{2}\ g_{a_0NN} \frac{f_{\pi NN}}{m_\pi} \frac{1}{s - m_N^2} F_N(s)$$
$$\times p_{1\mu}\ \bar{u}(p_2')\left[(p_1 + p_2)_\alpha \gamma_\alpha + m_N\right]\gamma_\mu\ \gamma_5 u(p_2), \qquad (39)$$
$$M_N^u\left(\pi^- p \to a_0^0 n\right) = \sqrt{2}\ g_{a_0NN} \frac{f_{\pi NN}}{m_\pi} \frac{1}{u - m_N^2} F_N(u)$$
$$\times p_{1\mu}\ \bar{u}(p_2')\gamma_\mu\gamma_5\left[(p_2 - p_1')_\alpha \gamma_\alpha + m_N\right] u(p_2), \qquad (40)$$

where $s = (p_1 + p_2)^2$, $u = (p_2 - p_1')^2$, m_N is the nucleon mass, $f_{\pi NN}^2/4\pi = 0.08$ [37]. The form factor for a virtual nucleon is taken as

$$F_N(u) = \left(\frac{\Lambda_N^4}{\Lambda_N^4 + (u - m_N^2)^2}\right)^j, \qquad (41)$$

where $j = 2$, Λ_N is the cut-off parameter chosen as $\Lambda_N = 1.3\,\mathrm{GeV}$. In ref. [30] it was found that the u-channel a_0-resonance contribution to the $\pi^+ p \to pK^+\bar{K}^0$ reaction calculated with the nucleon form factor $F_N(u)$ (41) of dipole type ($j = 2$) with $\Lambda_N \le 1.35\,\mathrm{GeV}$ is in reasonable agreement with existing experimental data.

Coming back to the amplitudes $A(s,t)$ and $B(s,t)$ defined by eq. (13) we find

$$A^{\{s\}}(s,t) = \sqrt{2}\ \left(s + m_N^2\right)\ g_{a_0NN} \frac{f_{\pi NN}}{m_\pi}\ \frac{F_N(s)}{s - m_N^2}\,,$$
$$B^{\{s\}}(s,t) = -\sqrt{2}\ 2m_N\ g_{a_0NN} \frac{f_{\pi NN}}{m_\pi}\ \frac{F_N(s)}{s - m_N^2} \qquad (42)$$

for the s-channel contribution and

$$A^{\{u\}}(s,u) = -\sqrt{2}\ \left(u + m_N^2\right)\ g_{a_0NN} \frac{f_{\pi NN}}{m_\pi}\ \frac{F_N(u)}{u - m_N^2}\,,$$
$$B^{\{u\}}(s,u) = \sqrt{2}\ 2m_N\ g_{a_0NN} \frac{f_{\pi NN}}{m_\pi}\ \frac{F_N(u)}{u - m_N^2} \qquad (43)$$

in the case of the u-channel mechanism.

In the case of the Regge-pole model with the ρ_2- and b_1-exchanges we have used the parametrization for $A(s,t)$ and $B(s,t)$ as suggested by Achasov and Shestakov [14]:

$$A^{\{\mathrm{Regge}\}}(s,t) \approx \frac{\gamma_{b_1}(t)}{\sqrt{s_0}} i \exp\left[-i\frac{\pi}{2}\alpha_{b_1}(t)\right]\left(\frac{s}{s_0}\right)^{\alpha_{b_1}(t)}, \qquad (44)$$

$$B^{\{\mathrm{Regge}\}}(s,t) \approx -\frac{\gamma_{\rho_2}(t)}{s} \exp\left[-i\frac{\pi}{2}\alpha_{\rho_2}(t)\right]\left(\frac{s}{s_0}\right)^{\alpha_{\rho_2}(t)}, \qquad (45)$$

where

$$\gamma_{\rho_2}(t) = \gamma_{\rho_2}(0)\ \exp(b_{\rho_2} t),$$
$$\gamma_{b_1}(t)\ = \gamma_{b_1}(0)\ \exp(b_{b_1} t),$$

and $s_0 \approx 1\,\mathrm{GeV}^2$. The meson Regge trajectories were taken in the linear form $\alpha_j(t) = \alpha_j(0) + \alpha_j'(0)t$. The parameters of the residues $\gamma_{\rho_2}(0)$, b_{ρ_2} and $\gamma_{b_1}(0)$, b_{b_1} were fixed in ref. [30] using the Achasov and Shestakov fit of the Brookhaven data on the $\pi^- p \to a_0^0 n$ reaction at $18\,\mathrm{GeV}/c$ [38]. They found two solutions with the relative b_1 contribution equal to 0 (fit 1) and 30% (fit 2). We use these two different choices of the Regge model for the analysis of the $\pi N \to a_0 N$ reaction.

We are very grateful to C. Hanhart for many useful discussions and clarifying remarks. This work was supported by DFG (grant 436 RUS 113/630) and by Russian Fund for Basic Research (grants 02-02-16783 and 03-02-04025).

References

1. D. Morgan, M.R. Pennington, Phys. Rev. D **48**, 1185 (1995).
2. V.V. Anisovich *et al.*, Phys. Lett. B **355**, 363 (1995).
3. L. Montanet, Nucl. Phys. B Proc. Suppl. **86**, 381 (2000).
4. V.V. Anisovich, L. Montanet, V.N. Nikonov, Phys. Lett. B **480**, 19 (2000).
5. S. Narison, Nucl. Phys. Proc. Suppl. **96**, 244 (2001).
6. J. Weinstein, N. Isgur, Phys. Rev. D **41**, 2236 (1990).
7. G. Janssen, B. Pierce, K. Holinde, J. Speth, Phys. Rev. D **52**, 2690 (1995).
8. J.A. Oller, E. Oset, Nucl. Phys. A **620**, 438 (1997); **652**, 407(E) (1999).
9. N.A. Törnqvist, Phys. Rev. Lett. **49**, 624 (1982).
10. E. van Beveren, G. Rupp, hep-ph/0304105.
11. R.J. Jaffe, Phys. Rev. D **15**, 267 (1997).
12. N.N. Achasov, S.A. Devyanin, G.N. Shestakov, Phys. Lett. B **88**, 367 (1979).
13. J. Vijande *et al.*, in *Proceedings of the International Workshop MESON 2002, Cracow, Poland* (World Scientific, Singapore, 2002), hep-ph/0206263.

14. N.N. Achasov, G.N. Shestakov, Phys. Rev. D **56**, 212 (1997).
15. T. Barnes, Phys. Lett. B **165**, 434 (1985).
16. O. Krehl, R. Rapp, J. Speth, Phys. Lett. B **390**, 23 (1997).
17. A.E. Kudryavtsev, V.E. Tarasov, JETP Lett. **72**, 410 (2000).
18. B.O. Kerbikov, F. Tabakin, Phys. Rev. C **62**, 064601 (2000).
19. F.E. Close, A. Kirk, Phys. Lett. B **489**, 24 (2000).
20. V.Yu. Grishina, L.A. Kondratyuk, M. Büscher *et al.*, Phys. Lett. B **521**, 217 (2001).
21. M. Büscher *et al.*, *Proceedings of the International Workshop Physics at COSY, Jülich, Aug. 28-Sept. 4, 2002*; hep-ph/0301126.
22. M. Büscher, *Proceedings of the XXVIII Mazurian Lakes Conference, Aug. 31-Sept. 6, 2003, Krzyze, Poland*; Acta Phys. Pol. B **35**, 1055 (2004).
23. V. Chernyshev *et al.*, COSY proposal #55, *Study of* a_0^+ *mesons at ANKE* (1997), available via www: `http://ikpd15.ikp.kfa-juelich.de:8085/doc/Anke.html`; L.A. Kondratyuk *et al.*, Preprint ITEP **18-97**, Moscow (1997).
24. M. Büscher *et al.*, *Beam-time request for COSY proposal #55 Study of* a_0^+ *mesons at ANKE* (2000), available via www: `http://ikpd15.ikp.kfa-juelich.de:8085/doc/Anke.html`.
25. M. Büscher *et al.*, *Status report for COSY experiment #55 Study of* a_0^+ *mesons at ANKE* and *Proposal Investigation of neutral scalar mesons* a_0^0/f_0 *with ANKE* (2001), available via www: `http://ikpd15.ikp.kfa-juelich.de:8085/doc/Anke.html`.
26. V. Kleber *et al.*, Phys. Rev. Lett. **25**, 172304 (2003).
27. E. Oset, J.A. Oller, U.-G. Meissner, Eur. Phys. J. **12**, 435 (2001).
28. V.Yu. Grishina, L.A. Kondratyuk, E.L. Bratkovskaya *et al.*, Eur. Phys. J. A **9**, 277 (2000).
29. E.L. Bratkovskaya, W. Cassing, L.A. Kondratyuk *et al.*, J. Phys. G **28**, 2423 (2002).
30. L.A. Kondratyuk *et al.*, Phys. At. Nucl. **66**, 155 (2003).
31. M.A. Abolins *et al.*, Phys. Rev. Lett. **25**, 469 (1970).
32. V.Yu. Grishina *et al.*, Phys. Lett. B **475**, 9 (2000).
33. V.Yu. Grishina, L.A. Kondratyuk, M. Büscher, Phys. At. Nucl. **63**, 1824 (2000).
34. A. Abele *et al.*, Phys. Rev. D **57**, 3860 (1998).
35. J. Cugnon, P. Deneye, J. Vandermeulen, Phys. Rev. C **41**, 1701 (1990).
36. A.A. Sibirtsev, W. Cassing, C.M. Ko, Z. Phys. A **358**, 101 (1997).
37. R. Machleidt, K. Holinde, Ch. Elster, Phys. Rep. **149**, 1 (1987); V. Mull, K. Holinde, Phys. Rev. C **51**, 2360 (1995).
38. A.R. Dzierba, in *Proceedings of the Second Workshop on Physics and Detectors for DA*Φ*NE'95, Frascati, 1995*, edited by R. Baldini *et al.*, Frascati Phys. Ser. **4**, 99 (1996).
39. C. Caso *et al.* (Particle Data Group), Eur. Phys. J. C **15**, 1 (2000).
40. V.Yu. Grishina *et al.*, Eur. Phys. J. A **10**, 355 (2001).
41. L.A. Kondratyuk *et al.*, Phys. Rev. C **48**, 2491 (1993).
42. V.Yu. Grishina *et al.*, Eur. Phys. J. A **19**, 117 (2004).
43. A.B. Kaidalov, Z. Phys. C **12**, 63 (1982).
44. A.B. Kaidalov, Surv. High Energy Phys. **13**, 265 (1999).
45. M. Guidal, J.M. Laget, M. Vanderhaeghen, Nucl. Phys. A **627**, 645 (1997).
46. A.C. Irving, R.P. Worden, Phys. Rep. **34**, 117 (1977).
47. A.B. Kaidalov, Sov. J. Nucl. Phys. **53**, 872 (1991).
48. C. Guaraldo, A.B. Kaidalov, L.A. Kondratyuk, Ye.S. Golubeva, Yad. Fiz. **59**, 1896 (1996); Phys. At. Nucl. **59**, 1395 (1996).
49. N. Kaiser, P.B. Siegel, W. Weise, Nucl. Phys. A **594**, 325 (1995); N. Kaiser, T. Waas, W. Weise, Nucl. Phys. A **612**, 297 (1997).
50. M.L. Goldberger, K.M. Watson, *Collision theory* (John Wiley and Sons, New York, 1964).
51. G. Fäldt, C. Wilkin, Nucl. Phys. A **587**, 769 (1995).
52. M. Lacomb *et al.*, Phys. Lett. B **101**, 139 (1981).
53. R.C. Barrett, A. Deloff, Phys. Rev. C **60**, 025201 (1999).
54. M. Torres, R.H. Dalitz, A. Deloff, Phys. Lett. B **174**, 213 (1986).
55. C. Hanhart, hep-ph/0311341.
56. A. Deloff, Phys. Rev. C **61**, 024004 (2000).
57. M. Kirchbach, D.O. Riska, Nucl. Phys. A **594**, 419 (1995).